induced upon deprotonation suggest that the same spin transfer mechanisms apply to the former complexes. If we assume a similar 30% decrease in dipolar shifts upon deprotonating PPFe(ImH)(CN), the Im^- contact shifts are also determined to be larger than the ImH contact shifts, with both the 2'- and 5'-positions exhibiting the opposite sign for proton and methyl group contact shifts.

Potential Protein Probes for the State of the Imidazole N_1H. The average heme methyl and 2,4-H shifts could, in principle, be used as a probe for determining the state of protonation of the axial histidyl imidazole(s) in low-spin ferric forms of hemoproteins. For most ferric cyano hemoproteins, only two or three of the needed resonances are resolved, making such analysis difficult. For ferricytochrome b_5, all four heme methyls are observed for the major component,[16,17] with the hyperfine shifts: 5-CH_3,21.8; 3-CH_3,14.4; 1-$CH_3$11.7; 8-CH_3,3.8 ppm; and 2-H, −28.2 and 4-H, −4.8 ppm for the deuterohemin reconstituted protein. The average shifts are as follows: CH_3, 13.2 ppm; 2,4-H, −16.5 ppm. These values compare better with 15.6 and −17.7 ppm for $[PPFe(ImH)_2]^+$, A, than with 9.7 and −11.8 ppm for $[PPFe(Im)_2]^-$, A'', indicating that in the major component of ferricytochrome b_5, the axial ligands most likely are neutral histidyl imidazoles, contrary to an earlier suggestion based on ESR data.[2]

From consideration of the chemical shifts of the axial imidazole protons in the present complexes, it seems reasonable to expect that the 2'-H of the axial histidyl imidazole ligand(s) in low-spin ferric hemoproteins should resonate upfield of the diamagnetic region irrespective of the state of protonation. In [PPFe(ImH)(CN)], C, 2'-H is observed at ~2 ppm, whereas in the deprotonated form, $[PPFe(Im)(CN)]^-$, C', it appears considerably upfield, particularly with 5'-CH_3Im^-. Therefore, the large shift change of 2'-H can be used as a probe of the state of protonation of the histidyl imidazole ligand.

For met-cyanomyoglobin, broad single-proton resonances have been detected[34] at ~19 and ~4 ppm which can be safely attributed to 4'-H and 2'-H of a neutral histidyl imidazole. In the cyanide complexes of horseradish peroxidase, HRP–CN, and cytochrome *c* peroxidase, CcP–CN, however, similar single-proton resonances are found[34] at approximately 16 ppm and −16 to −31 ppm. While proton NMR spectroscopy in H_2O solution has demonstrated[35] that there is an exchangeable proton associated in some manner with the axial imidazole, the large upfield bias for 2'-H has been interpreted[34] in terms of appreciable imidazolate character for the axial ligand, probably the result of strong hydrogen bonding of the N_1H to a glutamine side chain.[36] In contrast, the appearance[17] of 2'-H and 4'-H axial imidazole peaks in cytochrome b_5 at the positions expected for neutral ImH rather than Im^- argues against deprotonation of the axial ligand(s) in that protein. Although the magnitude of the 2'-H shift is not yet quantitatively interpretable in terms of the exact extent of hydrogen bonding, it appears that location and assignment of the 2'-H and 4'-H histidyl imidazole resonances in a variety of low-spin ferric cyano proteins by methods outlined elsewhere,[34] together with resonance Raman data on the iron–imidazole stretching frequency,[6,37,38] should lead to a more accurate description of the degree of hydrogen bonding in hemoproteins.

Acknowledgment. We thank J. S. Valentine for a preprint of her work. This research was supported by a grant from the National Institutes of Health, HL-16087, and by the UCD NMR Facility.

Registry No. DPFeCl, 21007-21-6; PPFeCl, 16009-13-5; deuterium, 7782-39-0; $[PPFe(ImH)_2]^+$, 25875-11-0; PPFe(Im)(ImH), 83603-96-7; $[PPFe(Im)_2]^-$, 83603-98-9; $[PPFe(CN)_2]^-$, 41127-52-0; PPFe(CN)(ImH), 33773-02-3; $[PPFe(CN)(Im)]^-$, 83603-97-8; $[DPFe(ImH)_2]^+$, 83603-99-0; $[DPFe(CN)_2]^-$, 52674-62-1; DPFe(CN)(ImH), 83604-00-6; $[DPFe(CN)(Im)]^-$, 83604-01-7; $[DPFe(Im)_2]^-$, 83604-02-8; $[PPFe(5'\text{-}CH_3ImH)_2]^+$, 83604-03-9; $[PPFe(5'\text{-}CH_3Im)_2]^-$, 83604-04-0; PPFe(CN)(5'-CH_3ImH), 83604-05-1; $[PPFe(CN)(5'\text{-}CH_3Im)]^-$, 83604-06-2; PPFe(CN)(2'-CH_3ImH), 83604-07-3; $[PPFe(CN)(2'\text{-}CH_3Im)^-$, 83604-08-4; 2'-$CH_3$ImH, 693-98-1; ImH, 288-32-4; KCN, 151-50-8.

(34) La Mar, G. N.; de Ropp, J. S.; Chacko, V. P.; Satterlee, J. D.; Erman, J. E. *Biochim. Biophys. Acta*, in press.
(35) de Ropp, J. S. Ph.D. Thesis, University of California, Davis, 1981.
(36) Poulos, T. L.; Kraut, J. *J. Biol. Chem.* **1980**, *255*, 8199–8205.
(37) La Mar, G. N.; de Ropp, J. S. *J. Am. Chem. Soc.* **1982**, *104*, 5203–5206.
(38) Teroaka, J.; Kitagawa, T. *J. Biol. Chem.* **1981**, *256*, 3969–3977.

Electronic States of the Quadruply Bonded $Re_2Cl_8^{2-}$ Species: An ab Initio Theoretical Study

P. Jeffrey Hay

Contribution from the Los Alamos National Laboratory, University of California, Los Alamos, New Mexico 87545. *Received February 16, 1982*

Abstract: The electronic structure of the "quadruply bonded" $Re_2Cl_8^{2-}$ species has been studied by using ab initio wave functions and relativistic effective core potentials. The metal–metal bonding in the ground state is discussed, and the rich spectrum of electronic states below 6 eV (50 000 cm^{-1}) is treated in detail, including correlation effects and spin–orbit coupling. Highly correlated multiconfiguration wave functions are needed to describe the electrons in the weak δ bond, particularly in the ground $^1A_{1g}$ state and the excited $^1A_{2u}$ (calculated 2.8 eV, experimental 1.8 eV), $^3A_{2u}$ (calculated 0.4 eV), and 2 $^1A_{1g}$ (calculated 3.2 eV) states. These excited states involving δ–δ^* excitations all undergo torsional distortions to D_{4d} geometries. The nature and relative intensities of weaker transitions involving excitations among the ten 5d orbitals as well as the strong transitions involving the Cl 3p–Re 5d charge-transfer excitations are also discussed.

The discovery of molecules with multiple metal–metal[1,2] bonds has stimulated numerous experimental and theoretical studies aimed toward understanding their electronic structure and spectral properties.[3–5] Calculations on such species have been carried out at the extended Huckel,[6,7] Xα scattered wave,[8,9] and ab initio levels.[10–14] The calculations to date have focused primarily on

(1) F. A. Cotton et al., *Science (Washington, D.C.)*, **145**, 1305 (1964).
(2) F. A. Cotton, *Inorg. Chem.*, **4**, 334 (1965).
(3) F. A. Cotton, *Acc. Chem. Res.*, **11**, 225 (1978).
(4) W. C. Trogler and H. B. Gray, *Acc. Chem. Res.*, **11**, 232 (1978).
(5) J. L. Templeton, *Prog. Inorg. Chem.*, **26**, 211 (1979).
(6) F. A. Cotton and C. B. Harris, *Inorg. Chem.*, **6**, 924 (1967).
(7) S. Shaik and R. Hoffmann, *J. Am. Chem. Soc.*, **102**, 1194 (1980).
(8) A. P. Mortola, J. W. Moskowitz, N. Rosch, C. D. Cowman, and H. B. Gray, *Chem. Phys. Lett.* **32**, 283 (1975).
(9) J. G. Norman and H. J. Kolari, *J. Am. Chem. Soc.*, **97**, 33 (1975).

0002-7863/82/1504-7007$01.25/0

the ground electronic states and on the states of the ions observed in photoelectron studies. These results have revealed that compared to "normal" bonds, the single configuration Hartree–Fock (HF) molecular orbital model of the metal–metal bond represents a less adequate description and that multiconfiguration wave functions are needed for an accurate picture of the bonding. In some cases the HF configuration may comprise only a small fraction of the total wave function.[11,14] In this paper the first detailed ab initio study of the electronic states of the $Re_2Cl_8^{2-}$ molecule, the now classic "quadruply bonded" species first characterized by Cotton and co-workers.[1,2] These calculations, carried out at the configuration interaction (CI) level on the basis of generalized valence bond (GVB) orbitals,[15,16] have been made possible by the development of relativistic effective core potentials.[17] These potentials enable one to incorporate into a one-electron potential (1) the effects of the core electrons and (2) the relativistic effects on the valence orbitals, which become substantial for third-row transition metals such as Re.[19] In addition, we explicitly include the effects of spin–orbit coupling by diagonalizing an effective spin–orbit operator over the CI wave functions. These calculations represent the first comprehensive treatment of the electronic states of a multiply bonded species to include correlation effects, relativistic effects, and spin–orbit coupling.

Details of the Calculation

Effective Core Potentials. For Re, the relativistic effective core potentials were derived according to the procedure discussed in earlier papers.[17,18] The s, p, and d ECP's were obtained by using the 5p, 5d, and 6s orbitals of the ^6D state of Re^{2+} having the configuration $(core)(5p)^6(5d)^4(6s)^1$ where "core" denotes $[Kr](5s)^2(4d)^{10}(4f)^{14}$. For the f and g potentials, for which there are no occupied valence orbitals of those symmetries, 5g and 5g orbitals in the presence of the "bare" (core) were used. The resulting potential was then represented in the usual form:

$$V = V_g + V_{s-g}|s><s| + V_{p-g}|p><p| + V_{d-g}|d><d| + V_{f-g}|f><f|$$

The nominally "core-like" 5p electrons were explicitly included here in light of our experience with other early-transition-metal and actinide molecules that have no nonbonding valence-electron pairs in the metal.[20] In such cases, ligands or another metal can approach sufficiently closely that the core–core overlap is no longer adequately represented by a point-change expression. In such cases, the inclusion of the outermost core shell has alleviated this problem.

For the Cl atoms, where a nonrelativistic ECP was used to represent the [Ne] core, the 3s and 3p orbitals were treated explicitly. The Gaussian expansions of the Re and Cl potentials are given in the supplementary material.

Basis Sets. A flexible basis of two contracted Gaussians to represent the valence 5d, 6s, and 6p orbitals of Re was chosen. The exponents were chosen to fit in a least-squares sense the pseudoorbitals of the Re^{2+} ion (chosen as a compromise between neutral Re and its formal valence of +3 in the complex). The 5p core electrons of Re and the 3s and 3p valence electrons of Cl were described by a minimal basis of contracted Gaussian functions. The Cl contraction coefficients were chosen on the basis of full "double-ζ" calculations in the $ReCl_4^-$ monomer. Details of the basis set are also given in the supplementary material section. Overall (3s5p4d) and (3s5p) primitive basis sets were contracted to [3s3p2d] and [1s1p] on the Re and Cl atoms, respectively.

GVB and CI Calculations. The orbitals for the GVB wave functions of the ground states of $Re_2Cl_8^{2-}$ (see next section) were obtained at the experimental bond geometry by using the GVBTWO program of Bobrowicz.[21] In all, 84 electrons were explicitly treated. The structural parameters from the X-ray diffraction studies[22] were as follows: R(Re–Re) = 2.24 Å, R(Re–Cl) = 2.29 Å, ∠Re–Re–Cl = 103.7°.

Virtual orbitals were obtained by removing a δ electron and solving for the excited orbitals in the presence of this field. Only the $4b_{1g}$ and $4b_{2u}$ orbitals corresponding to the combination of $5d_{x^2-y^2}$ orbitals (where the ligands have been chosen to lie in the xz and yz planes and the M–M bond defines the z axis) were found at low energies. The bulk of the calculations (GVB-CI) used the valence space of the ten 5d-like orbitals defined above. Additional POL-CI calculations, which utilized additional configurations having one electron in virtual orbitals, were also carried out. The results were very similar to the GVB-CI findings, and hence the discussion will focus almost entirely on the GVB-CI results.

The methodology of the CI calculations was as follows: Preliminary calculations for singlet and triplet states of each many-electron symmetry were used to identify the dominant configurations for each state within about 6 eV of the ground state. This often required several passes since practically all of the states have several important reference configurations. All single and double excitations were then generated within the valence space relative to this reference set. In addition, the lowest charge-transfer configurations were also identified.

Spin–Orbit Coupling. The effects of spin–orbit coupling on Re were incorporated by use of the one-electron, one-center model used successfully in our earlier studies.[23]

$$V_{so} = [Z_p^{eff}|p><p| + Z_d^{eff}|d><d|](l\cdot s)(r^{-3})$$

The values for Z^{eff} were chosen to reproduce the spin–orbit splittings in Re^{2+} as calculated from the relativistic numerical Hartree–Fock wave functions[24] by the Blume–Watson method. With the matrix elements of V_{so} calculated in the atomic basis, the matrix elements can then be computed for the basis of molecular orbitals. These in turn can be used to diagonalize the operator over the CI wave functions $(\Psi_{ASM_i}|V_{so}|\Psi_{BS'M'j})$ where A and B refer to the spatial symmetries, S and S' to the spin symmetries, M and M' to the M_S values, and i and j to the particular state of that symmetry. A more detailed presentation will be given in a forthcoming paper.

The Nature of the Quadruple Metal–Metal Bond and the δ–δ Electronic States

Theoretical Description of the Metal–Metal Bond. Historically[1,2] it was recognized immediately after the discovery of the $Re_2Cl_8^{2-}$ species that the four 5d electrons in each metal had the proper symmetries to be combined into one σ bond, two π bonds, and one δ_{xy} bond. Much discussion has centered on the relative strength of the four couplings in this and related species ranging from the strongly coupled molecular orbital (MO) picture to the weakly coupled valence-bond (VB) picture, which corresponds to antiferromagnetic metal–metal interactions when taken to the extreme weakly coupling limit. In the intervening years, experimental[3,4] studies of the chemistry and spectra of $Re_2Cl_8^{2-}$ and related species have filled in many details of the nature of the metal–metal bond, and a picture of a relatively robust Re–Re bond

(10) C. D. Garner, I. H. Hillier, M. F. Guest, J. C. Green, and A. W. Coleman *Chem. Phys. Lett.*, **48**, 587 (1976).
(11) A. Benard and A. Veillard, *Nouv. J. Chim.* **1**, 97 (1977).
(12) M. Benard, *J. Am. Chem. Soc.*, **100**, 2354 (1978).
(13) M. B. Hall, *J. Am. Chem. Soc.*, **102**, 2104 (1980).
(14) P. J. Hay, *J. Am. Chem. Soc.*, **100**, 2898 (1978).
(15) W. J. Hunt, P. J. Hay, and W. A. Goddard, III, *J. Chem. Phys.*, **57**, 738 (1972).
(16) T. H. Dunning, Jr., D. C. Cartwright, W. J. Hunt, P. J. Hay, and F. W. Bobrowicz, *J. Chem. Phys.*, **64**, 4755 (1976).
(17) P. J. Hay, W. R. Wadt, L. R. Kahn, and F. W. Bobrowicz, *J. Chem. Phys.*, **69**, 984 (1978).
(18) L. R. Kahn, P. J. Hay, and R. D. Cowan, *J. Chem. Phys.*, **68**, 2368 (1978).
(19) R. L. Martin and P. J. Hay, *J. Chem. Phys.*, **75**, 4539 (1981).
(20) (a) P. J. Hay, W. R. Wadt, L. R. Kahn, R. C. Raffenetti, and D. H. Phillips, *J. Chem. Phys.*, **70**, 1767. (b) W. R. Wadt, *J. Am. Chem. Soc.*, **101**, 6053 (1981).
(21) F. W. Bobrowicz and W. A. Goddard, III, in "Methods of Electronic Structure Theory", H. F. Schaefer, III, Ed., Plenum, New York, 1977.
(22) F. A. Cotton and C. B. Harris, *Inorg. Chem.*, **4**, 330 (1965).
(23) J. S. Cohen, W. R. Wadt, and P. J. Hay, *J. Chem. Phys.*, **71**, 2955 (1978).
(24) R. D. Cowan and D. C. Griffin, *J. Opt. Soc. Am.*, **66**, 1010 (1976).

has emerged with an estimated bond strength in the vicinity of 115–130 kcal/mol.[25]

Theoretical calculations[10-13] of multiply bonded metal–metal species of the first- and second-transition series have shown that the MO model often provides a poor quantitative description for 4d–4d bonds and a poor qualitative description for 3d–3d bonds! Highly correlated multiconfiguration wave functions are needed to give a reasonable description of the bonding in these molecules. Practically all the theoretical activity has centered on ground electronic states of metal–metal bonds. Furthermore, the number of electrons and the importance of relativistic effects have precluded ab initio calculations on molecules involving third-row transition metals until the advent of relativistic effective core potentials.

In this paper we give an extensive treatment of the ground and all low-lying excited states below 6 eV (50 000 cm^{-1}) of the $Re_2Cl_8^{2-}$ species using correlated wave functions. (A preliminary account of the results for the ground state and several excited states of $Re_2Cl_8^{2-}$ has been given elsewhere.[14]) Before discussing these states in detail we shall first discuss the bonding in the ground state in terms of the simple conceptual basis offered by the generalized valence bond scheme and the implications it suggests for discussing the δ–δ^* excitations of the molecule.

In the GVB approach,[15,16] instead of describing an electron pair in a bond by a pair of identical orbitals $\phi_i(1)\bar{\phi}_i(2)$, each electron is described by a separate orbital $\phi_{ia}(1)\bar{\phi}_{ib}(2) + \phi_{ib}(1)\bar{\phi}_{ia}(2)$ where $\langle\phi_{ia}|\phi_{ib}\rangle \neq 0$. Each of the four bonds in $Re_2Cl_8^{2-}$ is described in an analogous manner, and the total wave function has the form

$$\Psi_{GVB} = A\Psi_{core}(\phi_{\sigma a}\bar{\phi}_{\sigma b} + \phi_{\sigma b}\bar{\phi}_{\sigma a})(\phi_{\pi xa}\bar{\phi}_{\pi xb} + \phi_{\pi xb}\bar{\phi}_{\pi xa}) \times (\phi_{\pi ya}\bar{\phi}_{\pi yb} + \phi_{\pi yb}\phi_{\pi ya})(\phi_{\delta a}\bar{\phi}_{\delta b} + \phi_{\delta b}\bar{\phi}_{\delta a}) \quad (1)$$

where A is the antisymmetrizer and Φ_{core} represents the doubly occupied orbitals of the Cl ligands. The GVB wave function can

$$\Phi_{core} = ...(3a_{1g})^2(3a_{2u})^2(1a_{2g})^2(1a_{1u})^2(3b_{1g})^2\text{-}(3b_{2u})^2(1b_{2g})^2(1b_{1u})^2(4e_u)^4(4e_g)^4 \quad (2)$$

be cast into the orthogonal "natural orbital" (NO) representation where the pairs are written as $c_1\phi_{i1}(1)\bar{\phi}_{i1}(2) - c_2\phi_{i2}(1)\bar{\phi}_{i2}(2)$ where $\langle\phi_{i1}|\phi_{i2}\rangle = 0$ and $(c_1)^2 + (c_2)^2 = 1$. In this representation the wave function has the form

$$\Phi_{GVB} = A\Phi_{core}[c_1(4a_{1g})^2 - c_2(4a_{2u})^2][c_3(5e_{ux})^2 - c_4(5e_{gx})^2] \times [c_3(5e_{uy})^2 - c_4(5e_{gy})^2][c_5(2b_{2g})^2 - c_6(2b_{1u})^2] \quad (3)$$

We will also adopt the familiar designation for the orbitals as follows:

$$\sigma \sim 4a_{1g} \qquad \sigma^* \sim 4a_{2u}$$
$$\pi_x \sim 5e_{ux} \qquad \pi_x^* \sim 5e_{gx}$$
$$\pi_y \sim 5e_{ux} \qquad \pi^* \sim 5e_{gy}$$
$$\delta \sim 2b_{2g} \qquad \delta^* \sim 2b_{1u}$$

Setting $c_2 = c_4 = c_6 = 0$ in the above wave function produces the Hartree–Fock (HF) wave function. Although one sometimes refers to the ground state in terms of the HF "$\sigma^2\pi^4\delta^2$" configuration, we shall discuss below the limitations of this designation, particularly for the δ bond. In addition, we demonstrate how the GVB description leads to a straightforward explanation of the ordering of the ground and δ–δ^* states of $Re_2Cl_8^{2-}$.

The GVB orbitals (eq 1) for $Re_2Cl_8^{2-}$ are plotted in Figure 1 where the σ orbitals are seen to be predominantly d_{z^2} orbitals on each metal atom with significant delocalization onto the other metal. The π orbitals, mostly $5d_{xz}$ in character on a given metal, show less delocalization, and the δ orbitals are essentially $5d_{xy}$ orbitals entirely localized on each center. These trends are reflected in the steady decrease in overlap of the GVB orbitals (see Table I) σ (0.67) > π (0.47) ≫ δ (0.13). The HF orbitals, which are required to have overlaps of 1.0, are thus progressively poorer descriptions of the σ, π, and δ bonds of the system.

Table I. Analysis of the Orbitals Involved in the Metal-Metal Bond of $Re_2Cl_8^{2-}$ in the Orthogonal Natural Orbital (NO) and Nonorthogonal VB Representation of the Ground-State GVB Wave Function

orbital	Hartree-Fock[a]	GVB-PP[b]	GVB-CI[c]
Pair Overlaps–VB Representation			
σ_a, σ_b	1.0	0.672	
π_{xa}, π_{xb}	1.0	0.566	
π_{ya}, π_{yb}	1.0	0.566	
δ_a, δ_b	1.0	0.130	
total bond order		1.934	
Occupation Numbers–NO Representation			
σ	2.0	1.924	1.808
π_x	2.0	1.854	1.800
π_y	2.0	1.854	1.800
δ	2.0	1.254	1.392
δ^*	0.0	0.746	0.608
π^*_y	0.0	0.146	0.200
π^*_y	0.0	0.146	0.200
σ^*	0.0	0.076	0.192

[a] One configuration. [b] Sixteen configurations. [c] 526 configurations.

The more highly correlated nature of the δ bond is also apparent in the occupation numbers (f_k) of the orthogonal natural orbitals (Table I). These are defined in terms of the CI coefficients (c_k) in eq 3.

$$f_k = 2c_k^2$$

The occupation numbers, which would be 2.0 and 0.0 for the bonding and antibonding orbitals, respectively, in the HF wave function, turn out to be 1.4 and 0.6 for the δ and δ^* orbitals. This is one indication of the marked departure from the molecular orbital picture. The $\sigma^2\pi^4\delta^2$ configuration represents only 55% of the total wave function for the ground state of $Re_2Cl_8^{2-}$.

δ–δ^* Excited States. From the δ and δ^* MO's, one can construct four possible electronic states as follows: two $^1A_{1g}$ states—$(\delta)^2$ and $(\delta^*)^2$; a $^1A_{2u}$ state—$(\delta)^1(\delta^*)^1$, and a $^3A_{2u}$ state—$(\delta)^1(\delta^*)^1$. In the traditional MO approach, one would expect the following ordering:

$$^1A_{1g}(\delta)^2 \ll {}^3A_{2u}(\delta\delta^*) < {}^1A_{2u}(\delta\delta^*) \ll {}^1A_{1g}(\delta^*)^2$$
(MO model)

on the basis of the relative energies of bonding and antibonding orbitals.

The extremely localized nature of the GVB δ_a and δ_b orbitals ($S_{ab} = 0.13$) suggests an alternative valence bond interpretation of the four states. In terms of these GVB orbitals, the ground state ($1^1A_{1g} = A(\delta_a\bar{\delta}_b + \delta_b\bar{\delta}_a)$) is very close to the VB limit where δ_a and δ_b would be purely atomic d_{xy} orbitals on each center. In such a limit, the triplet coupling of these orbitals will be only slightly higher in energy ($^3A_{2u} = A(\delta_a\bar{\delta}_b - \delta_{ba}\bar{})$), and in the limit where the overlap $S_{ab} \to 0$, the singlet and triplet states become degenerate.

The other states then correspond to "ionic" configurations, with both δ electrons on a given metal: $^1A_{2u} = A(\delta_a\bar{\delta}_a - \delta_b\bar{\delta}_b)$; $2^1A_{1g} = A(\delta_a\bar{\delta}_a + \delta_b\bar{\delta}_b)$. In the case of $Re_2Cl_8^{2-}$, where each Re formally has a $(5d)^4$ configuration and +3 charge, the first two states correspond to a Re^{3+}–Re^{3+} situation while the last two states would have Re^{2+}–Re^{4+} character. Thus the latter two would lie at higher energies with the ordering $^1A_{2u} < 2^1A_{1g}$ since the two $^1A_{1g}$ states can interact. Overall this valence bond model would predict the overall or dering

$$1^1A_{1g} < {}^3A_{2u} \ll {}^1A_{2u} < 2^1A_{1g} \qquad \text{(VB model)}$$

This is the same order of states suggested from the MO model, but the relative spacing differs markedly in the VB model. These two viewpoints represent the extremes spanned by chemical bonds in molecules—approaching the MO view in the high overlap ($S_{ab} \to 1$) limit and approaching the VB view in the low overlap ($S_{ab} \to 0$) limit.

(25) W. C. Trogler, C. D. Cowman, H. B. Gray, and F. A. Cotton, *J. Am. Chem. Soc.*, **99**, 2993 (1977).

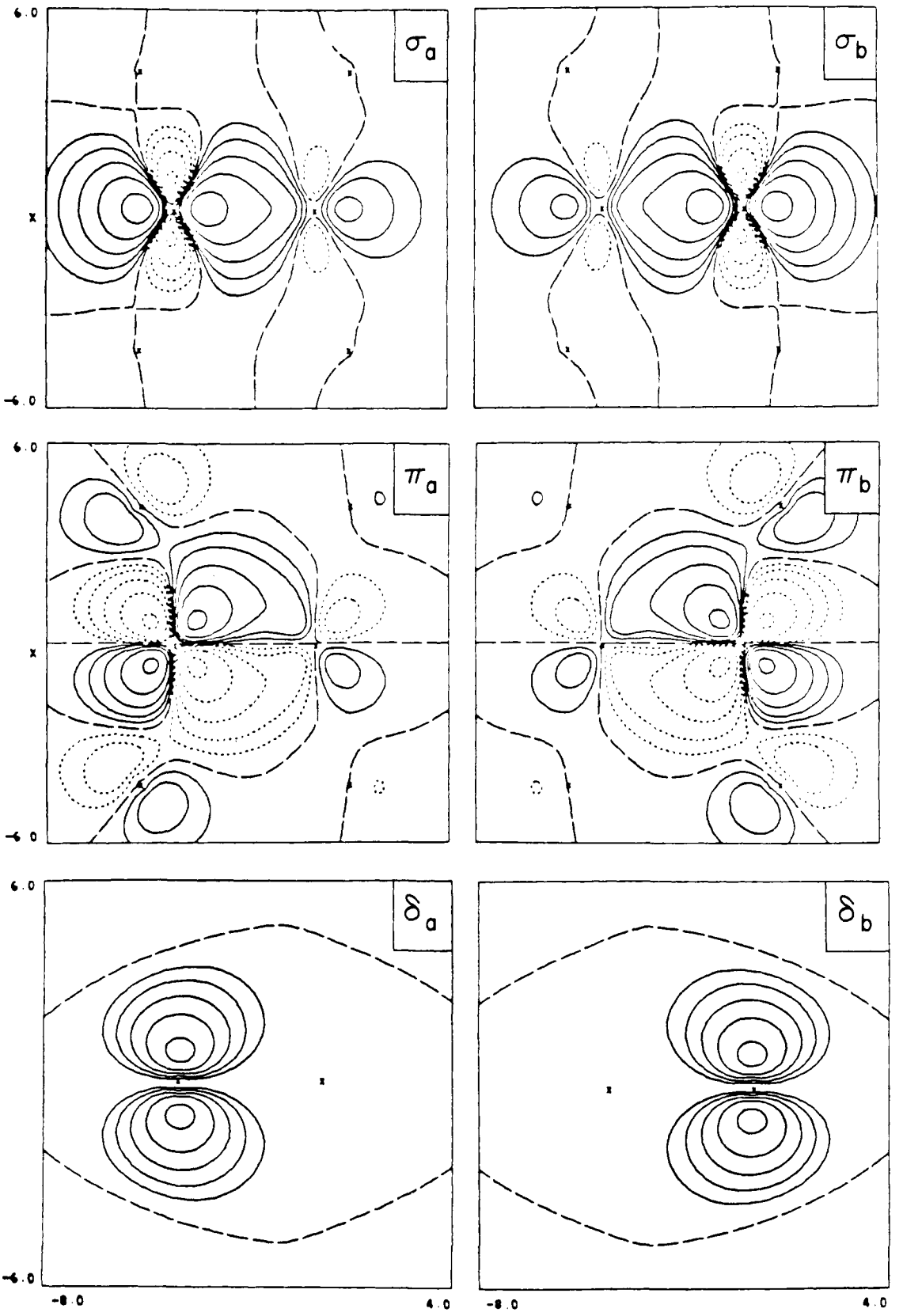

Figure 1. Contour plots of the GVB orbitals involved in the σ, π, and δ bonds of $Re_2Cl_8^{2-}$. Positive, zero and negative contours are denoted by solid, dashed, and dotted lines, respectively; ×'s denote positions of the nuclei. The σ and π orbitals are plotted in the xz plane; the δ orbitals are plotted in a plane rotated 45° relative to the xz plane.

This qualitative picture of the ordering of states from the VB model is borne out by the CI results shown in Table II and Figure 2. The GVB-CI and full 8e-CI results utilize the eight ground-state orbitals while the POL-CI involves the orbitals plus virtual orbitals. The GVB-CI includes many double and quadruple excitations from the $\sigma^2\pi^4\delta^2$ configuration while the full Ci includes up to octuple excitations. The ordering $1^1A_{1g} < {}^3A_{2u} \ll {}^1A_{2u} < 2^1A_{1g}$ is similar for the various types of CI calculations. The POL-CI calculations predict the triplet state to lie only 0.4 eV (3200 cm^{-1}) above the ground state. The dipole-allowed $^1A_{2u}$ state is found at 2.8 eV (22 400 cm^{-1}), or about 1.0 eV higher than the observed band at 1.8 eV (under Comparison with Experimental

Table II. Selected Low-Lying States of $Re_2Cl_8^{2-}$ as a Function of Various Levels of CI Calculations

state	overall designtn	excitation energy, eV GVB-PP	GVB-CI	POL-CI	full 8e-CI
1^1A_{1g}			0.00	0.00	0.00
1^3A_{2u}	δ-δ^*		0.75	0.40	0.36
1^1A_{2u}	δ-δ^*		3.20	2.85	3.25
2^1A_{1g}	$\delta\delta$-$\delta^*\delta^*$		3.40	3.22	3.54
1^1E_g	π-δ^*		3.87	3.54	
2^1E_g	δ-π^*		4.76	4.40	
		total energy (E + 226 au)			
1^1A_{1g}		−0.794 37	−0.850 49	−0.856 42	−0.868 26

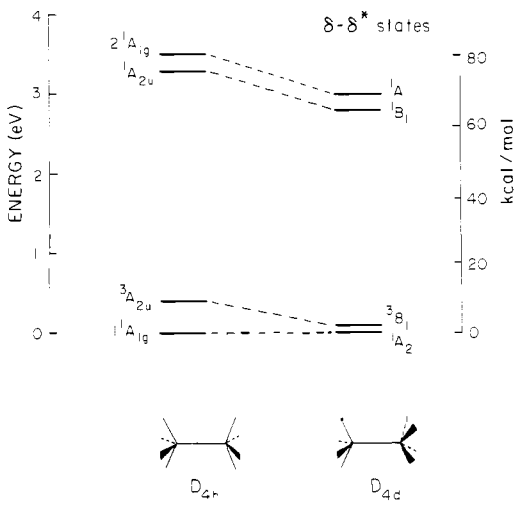

Figure 2. Calculated energies of the electronic states of $Re_2Cl_8^{2-}$ involving δ-δ^* excitations (from full 8e-CI results). Also shown is the correspondence between the states for the eclipsed (D_{4h}) and staggered (D_{4d}) geometries.

Spectra). The 2^1A_{1g} state lies still higher (3.2 eV) in energy. In view of both the large separation (over 2 eV) between $^1A_{2u}$ and $^3A_{2u}$ δ-δ^* states and the qualitative difference in the nature of the states, calculations such as Xα scattered wave, which give an average δ-δ^* excitation energy, should not be expected to give estimates for the location of the $^1A_{2u}$ state itself but rather for some weighted average of the singlet and triplet states. The average transition energy for the δ-δ^* excitation was found to be 4488 cm^{-1} (0.5 eV) from an Xα scattered wave calculation,[8] or 1.23 eV below observed peak and quite close in energy to our calculated value for the $^3A_{2u}$ state.

The overestimate of the δ-δ $^1A_{2u}$ excitation energy is not surprising in view of the experience to date in describing analogous ionic states, or "V-like" states in Mulliken's notation,[26] in hydrocarbon molecules. Such states are characterized by large correlation and polarization effects associated with their C^+–C^- nature.

All four of the states in the δ-δ^* manifold have large contributions from more than one configuration (Table III). Thus the designation of these excited states as δ-δ^*, δ-δ^*, and $\delta\delta$-$\delta^*\delta^*$ for $^3A_{2u}$, $^1A_{2u}$, and 2^1A_{1g}, respectively, has at most only qualitative significance.

Although we shall return to the question of intensities of the absorption bands in a later section, the highly localized nature of the δ orbitals in the ground state accounts for the low intensity of the $^1A_{1g} \rightarrow {}^1A_{2u}$ absorption band. The oscillator strength for an electronic transition involving nondegenerate states is given by

$$f = 8\pi^2 m e \bar{\nu} |\mu_{ij}|^2 / 3h = 1.096 \times 10^{11}\, \nu(\mathrm{cm}^{-1}) |\mu_{ij}(\mathrm{cm})|^2$$

where

$$\mu_{ij} = \int \Psi^*_j q \Phi_i \, d\tau \qquad q = x, y, \text{ or } z$$

If the ground and excited states were described in the MO picture as $(\delta)^2$ and $(\delta)^1(\delta^*)^1$, respectively, Mulliken showed that[26]

$$\mu_{ij} \approx R/2(1 - S^2)^{1/2} \qquad \text{(MO description)}$$

while if they were described in terms of the "covalent" and "ionic" VB states

$$\mu_{ij} \approx SR \qquad \text{(VB description)}$$

where S is the atomic orbital overlap integral and R is the intermolecular separation. The VB description would lead to significantly reduced oscillator strengths if $S < 0.5$. Trogler et al.[27] inferred that an overlap of 0.1, quite close to the δ overlap of 0.13 calculated here, would account for the observed f value of 0.023 in $Re_2Cl_8^{2-}$.

In terms of the orthogonal NO representation of the GVB wave function, if the two states are represented as

$$^1A_{1g}: \quad c_1(\delta)^2 - c_2(\delta^*)^2$$

$$^1A_{2u}: \quad [\delta\bar{\delta}^* + \delta^*\bar{\delta}]/2^{1/2}$$

the transition moment becomes

$$\mu_{ij} = (^1A_{2u}|z|^1A_{1g}\rangle = \langle\delta|z|\delta^*\rangle(c_1 - c_2)/2^{1/2}$$

Using the calculated value of $\delta|z|\delta^*\rangle = 2.2$ au (1 au = 0.520 × 10^{-8} cm) and values of 0.86 and 0.50 for c_1 and c_2 yields a considerably reduced $\mu_{ij} = 0.44$. The value for μ_{ij} from the actual CI wave functions is even smaller (0.24), indicating that other correlation effects also serve to reduce the magnitude.

Eclipsed and Staggered Conformations. Another indication of the strength of the quadruple bond is the barrier to rotation about the bond. We considered the eclipsed (D_{4h}) and staggered (D_{4d}) forms by varying only the torsional angle of the ligands about the axis and keeping all other geometrical parameters fixed.

The relationship between the electronic states of the two forms is most easily seen in the valence bond representation:

	D_{4h}	D_{4d}
$^1A_{1g}$:	$\delta_a\bar{\delta}_b + \delta_b\bar{\delta}_a$	$\rightarrow {}^1B_2$
$^3A_{2u}$:	$\delta_a\delta_b$	$\rightarrow {}^3B_1$
$^1A_{2u}$:	$\delta_a\bar{\delta}_b - \delta_b\bar{\delta}_b$	$\rightarrow {}^1B_2$
$^1A_{1g}$:	$\delta_a\bar{\delta}_a + \delta_b\bar{\delta}_b$	$\rightarrow {}^1A_1$

In D_{4h} symmetry, δ_a and δ_b refer to d_{xy} on both centers; in D_{4d} symmetry, δ_a is d_{xy} and δ_b is $d_{x^2-y^2}$ if we treat the ligands of center B as having rotated by 45°. The orbitals describing the other six electrons of the bond are axially symmetric overall and need not be considered here.

The results of the full eight-electron GVB-CI calculations (shown in Figure 2) indicate essentially no preference for the ground state for either geometry since there is essentially no barrier to rotation (less than 1 kcal/mol). Also, at the staggered geometry, the singlet ($^1A_2$) and triplet ($^3B_1$) states have become nearly degenerate. Although the present calculations are unlikely to be reliable to within 1 kcal/mol, it is perhaps surprising that we find no inherent stabilization of the eclipsed form observed experimentally. In stating that the rotational barrier must be quite small, we should also mention the possibility that a stronger preference for the eclipsed geometry might have been found had we included either (1) f polarization functions in the basis to provide a more accurate description of the δ bond or (2) a more flexible Cl atom basis. Finally there is the question of translating the present results of a dianion in vacuo to the observed geometries in solution or in the crystal.

These puzzling results for the rotational barrier are similar to the findings of Benard,[12] who examined the rotational barrier of the quadruply bonded $Mo_2Cl_8^{4-}$ species. Although it is known

(26) R. S. Mulliken, *J. Chem. Phys.*, **7**, 20 (1939).

(27) W. C. Trogler, E. I. Solomon, I. Trajberg, C. J. Ballhausen, and H. B. Gray, *Inorg. Chem.*, **16**, 828 (1977).

Table III. Dominant Configurations for Selected States of $Re_2Cl_8^{2-}$

state	overall designtn	CI coeff	occupation numbers									
			σ	π_x	π_y	δ	δ^*	π^*_x	π^*_y	σ^*	δ_{xy}	δ^*_{xy}
1^1A_{1g}	$[\sigma^2\pi^4\delta^2]$	0.79	2	2	2	2	0	0	0	0	0	0
		−0.46	2	2	2	0	2	0	0	0	0	0
		−0.12	2	2	0	2	0	0	2	0	0	0
		−0.12	2	0	2	2	0	2	0	0	0	0
1^3A_{2u}	δ–δ^*	0.92	2	2	2	1	1	0	0	0	0	0
		−0.13	2	1	2	2	0	1	0	0	0	0
		−0.13	2	2	1	2	0	0	1	0	0	0
1^1A_{2u}	δ–δ^*	0.85	2	2	2	1	1	0	0	0	0	0
		−0.24	2	1	2	2	0	1	0	0	0	0
		−0.24	2	2	1	2	2	0	1	0	0	0
		−0.19	2	1	2	0	2	1	0	0	0	0
		−0.19	2	2	1	0	2	0	1	0	0	0
2^1A_{1g}	$\delta\delta$–$\delta^*\delta^*$	0.71	2	2	2	0	2	0	0	0	0	0
		0.45	2	2	2	2	0	0	0	0	0	0
		−0.29	2	1	2	1	1	1	0	0	0	0
		−0.29	2	2	1	1	1	0	1	0	0	0
1^1A_{2g}	δ–δ_{xy}	0.77	2	2	2	1	0	0	0	0	1	0
		−0.52	2	2	2	0	1	0	0	0	1	0
1^1E_g	π–δ^*	0.88	2	2	1	2	1	0	0	0	0	0
		−0.25	2	2	2	1	0	1	0	0	0	0
2^1E_g	δ–π^*	0.90	2	2	2	1	0	1	0	0	0	0
		0.23	2	2	1	2	1	0	0	0	0	0

experimentally to assume the eclipsed D_{4h} geometry, SCF calculations predicted the triplet state of the staggered D_{4d} form to be more stable by 60 kcal! This turns out to be more a reflection of the inadequacy of the SCF description of the δ bond in the eclipsed form, since the triplet state is more reasonably represented by a single configuration. CI calculations by Benard reduced this apparent barrier to 4 kcal/mol, but still in favor of the staggered form, which is to be compared with the negligible barrier (<1 kcal) computed here for $Re_2Cl_8^{2-}$.

The $^3A_{2u}$ and $^1A_{2u}$ states of the D_{4h} form show a pronounced preference (by 8 and 5 kcal/mol, respectively) for the staggered geometry. The situation is quite reminiscent of the states of the double bond in ethylene[28] where the π–π^* triplet (T) state becomes stabilized and essentially degenerate with the ground state for 90° twist angle and where the π–π^* singlet (V) state also shows a pronounded tendency to twist away from the planar form.

The preference for staggered geometries by the $^1A_{2u}$ state is consistent with emission studies on $Re_2Cl_8^{2-}$ and related species by Gray and co-workers.[29,30] The large shift in the emission band from the $^1A_{2u}$ absorption peak and the lack of mirror symmetry between the bands suggested either emission from the $^3A_{2u}$ state or a highly distorted excited state. Later studies[30] ruled out the presence of a triplet state close to the $^1A_{2u}$ state and favored instead a D_{4d} distortion in the excited state leading to poor Franck–Condon overlap with the ground state. The sterically hindered $Mo_2Cl_4(PBu_3)_4$ complex in fact showed vibronically structured emission that did mirror the absorption band. The bulky phosphine groups served to prevent the excited state from attaining the D_{4d} geometry achieved in $Re_2Cl_8^{2-}$ and hence maintain good Franck–Condon overlap with the ground state.

Nature of the Higher Electronic States

The four lowest excited states discussed above represent all possible couplings of the electrons in the δ and δ^* orbitals. The higher d–d electronic states must then necessarily involve excitations either out of the 5d bonding (σ or π) orbitals or into the antibonding (σ^* or π^*) orbitals. In addition, the formally unoccupied $5d_{x^2-y^2}$ orbitals on each Re provide low-lying virtual orbitals ($4b_{1g}$, $4b_{2u}$—designated here as δ' and δ'^*) for excitations. Finally the lowest ligand-to-metal charge-transfer (CT) states will arise from exciting the highest lying orbitals of Cl 3p parentage into the δ^* orbitals. Although the ensuring classification of states by such designations as π–δ^* imply a MO-like framework, we should reemphasize the inadequacies of such a description especially for the δ and δ^* orbitals. The near degeneracy of these orbitals (or, in VB language, the weak coupling of the d_{xy} orbitals) results in the situation where nearly all the states of $Re_2Cl_8^{2-}$ have two or more important configurations (see Table III). For purposes of nomenclature, we will denote each state by its most important configuration and, where possible, also give a VB in-

Table IV. Electronic States of $Re_2Cl_8^{2-}$ without Spin-Orbit Coupling from CI Calculations

dominant configuration	singlet states		triplet states	
	symmetry	ΔE, eV	symmetry	ΔE, eV
$[\sigma^2\pi^4\delta^2]$	1^1A_{1g}	0.00		
δ–δ^*	1^1A_{2u}	3.20	1^3A_{2u}	0.75
$\delta\delta$–$\delta\delta^*$	2^1A_{1g}	3.40		
π–δ^*	1^1E_g	3.87	1^3E_g	3.16
δ–π^*	2^1E_g	4.76	2^3E_g	4.17
$\pi\delta$–$\delta^*\delta^*$	1^1E_u	4.79	1^3E_u	4.00
$\delta\delta$–$\delta^*\pi^*$	2^1E_u	5.83	2^3E_u	5.01
π–π^*	2^1A_{1u}	5.50	2^3A_{2u}	3.84
	1^1B_{2u}	5.92	1^3B_{1u}	4.52
	2^1B_{1u}	5.99	1^3B_{2u}	4.64
	1^1A_{2u}	7.48	2^3A_{1u}	5.47
δ–δ'	$^1A_{2g}$	4.71	$^3A_{2g}$	4.76
δ–δ'^*	$^1A_{1u}$	4.82	$^3A_{1u}$	4.92
σ–δ^*	1^1B_{1u}	5.30	2^3B_{1u}	5.26
σ–π^*	3^1E_g	6.84	3^3E_g	5.91
$\pi\delta$–$\delta^*\pi^*$	3^1A_{1g}	5.70	1^3A_{1g}	5.07
	1^1B_{2g}	5.95	1^3B_{2g}	5.36
	1^1B_{1g}	6.35	2^3A_{2g}	4.70
	4^1A_{1g}	6.59	1^3B_{1g}	5.93
LMCT				
a_{1u}–$\delta^*(b_{1u})$	2^1B_{1g}	6.35	2^3B_{1g}	6.05
b_{2u}–δ^*	2^1A_{2g}	6.35	4^3A_{2g}	6.22
a_{2g}–δ^*	2^1B_{2u}	6.53	2^3B_{2u}	6.31
e_g–δ^*	3^1E_u	6.81	4^3E_u	6.63
e_g–δ^*	4^1E_u	6.93	5^3E_u	6.81
e_u–δ^*	4^1E_g	7.09	4^3E_g	

(28) R. J. Buenker and S. D. Peyerimhoff, *Chem. Phys.*, **9**, 75 (1975).
(29) W. C. Trogler, E. I. Solomon, and H. B. Gray, *Inorg. Chem.*, **16**, 3031 (1977).
(30) V. M. Miskowski, R. A. Goldbeck, D. S. Kliger, and H. B. Gray, *Inorg. Chem.*, **18**, 86 (1979).
(31) K. P. Huber and G. Herzberg in "Molecular Spectra and Molecular Structure, IV. Constants of Diatomic Molecules", Van Nostrand Reinhold, New York, 1979.

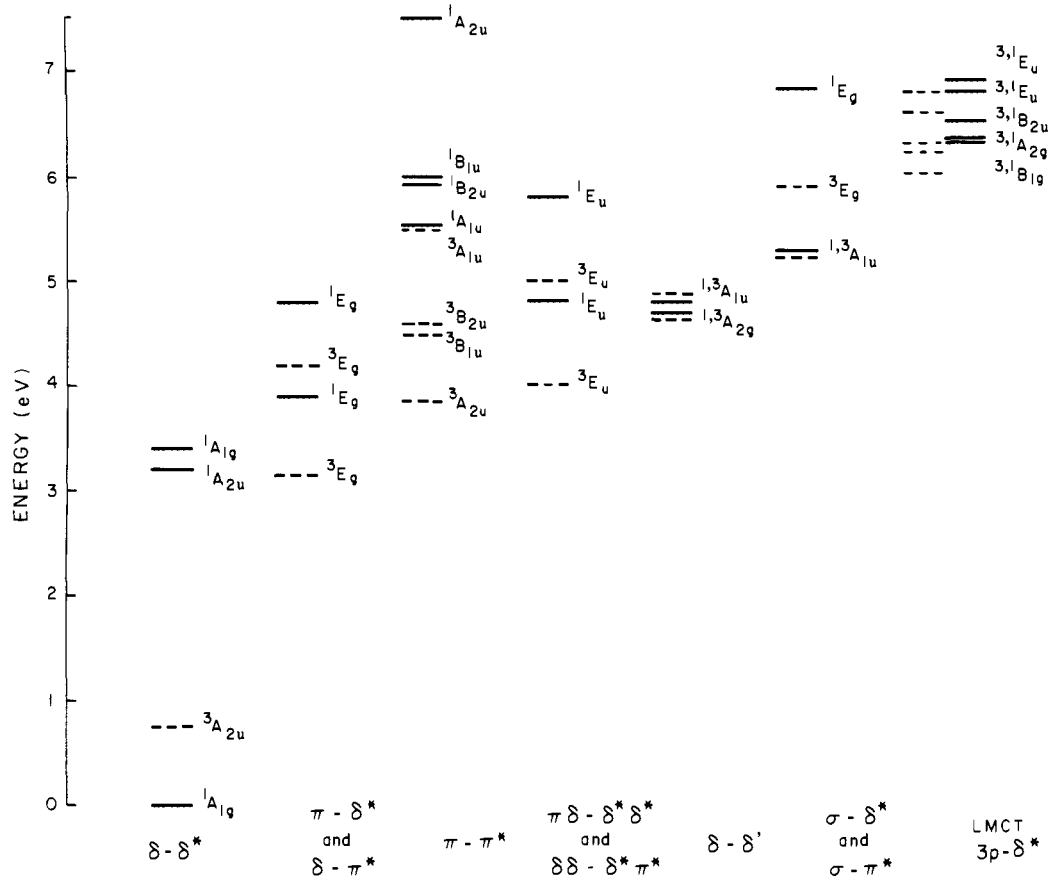

Figure 3. Calculated electronic states of $Re_2Cl_8^{2-}$ without spin–orbit coupling (GVB-CI results). Singlet and triplet states are denoted by solid and dashed lines, respectively. The states are grouped by families of common parentage according to the orbital excitations shown at the bottom.

terpretation to the classification of electronic states.

The rich manifold of excited electronic states in $Re_2Cl_8^{2-}$ is shown in Figure 3 where they have been classified in blocks according to their orbital parentage. A particular excitation (π–π^*, for example) can give rise to a manifold containing as many as eight many-electron singlet or triplet states separated in energy by several electronvolts. Further details on the excitation energies are given in Table V. The orbital excitations used to classify the states refer to the nominal ground-state configuration $(\sigma)^2(\pi)^4(\delta)^2$. Hence states denoted as π–π^* and $\pi\delta$–$\pi^*\delta^*$ would have dominant configurations $(\sigma)^2(\pi)^3(\delta)^2(\pi^*)^1$ and $(\sigma)^2(\pi)^3(\delta^*)^1(\pi^*)^1$, respectively. The nature of the electronic states is discussed below in detail.

δ–δ' States. In addition to the $^{1,3}A_{2u}$ and $^1A_{1g}$ states arising from the δ–δ^* and $\delta\delta$–$\delta^*\delta^*$ excitations, respectively, one also finds $^1A_{2g}$, $^3A_{2g}$, $^1A_{1u}$, and $^3A_{1u}$ states at higher energies (4.7–4.9 eV) corresponding to the δ–δ' and δ–δ'^* excitations. If each metal atom can be thought of having an atomic $(d_{z^2})^1(d_{xz})^1(d_{yz})^1(d_{xy})^1$ configuration (M), these states would correspond to excitation of one metal atom to a $(d_{z^2})^1(d_{xz})^1(d_{yz})^1(d_{x^2-y^2})^1$ configuration (M*). The many-electron A_{2g} and A_{1u} states are constructed from linear combinations of the VB configurations M*M ± MM*. Reexpression of this representation into MO configurations requires two configurations to describe each state, as was the case for the $^1A_{1g}$ ground state. For example (see Table III), the $^1A_{2g}$ state contains strong admixtures of δ–δ' and δ^*–δ'^* excitations. At much higher energies, there should also exist another $^1A_{2g}$ state (not shown here) arising from the other combination of these two configurations and corresponding to the excitation of a d_{xy} orbital on center A to a $d_{x^2-y^2}$ orbital on center B producing a molecular Re^{2+}–Re^{4+} state analogous to the δ–δ^* 1^1A_{2u} state.

π–δ^* and δ–π^* States. The ^1E_g (3.87 eV) and ^3E_g (3.16 eV) states arising from the π–δ^* excitation are the lowest calculated states in $Re_2Cl_8^{2-}$ that do not involve the δ–δ^* manifold. At slightly higher energies are the δ–π^* ^1E_g and ^3E_g states (4.76 and 4.17 eV) of the same symmetry.

In addition, in this vicinity there are two pairs of states with ^1E_u and ^3E_u symmetries. In MO language, these E_u states correspond to double excitations. The first $^{1,3}E_u$ pair (at 4.8 and 4.0 eV) arises from a π–δ^* excitation—the same excitation producing the first ^1E_g and ^3E_g pair—coupled with a δ–δ^* excitation, denoted here as $\pi\delta$–$\delta^*\delta^*$ overall. The higher $^{1,3}E_u$ pair (5.0 eV) stems from the δ–π^* and δ–δ^* double excitation, or $\delta\delta$–$\delta^*\pi^*$, analogous to the second E_g pair.

In VB language, these states can again be seen as linear combinations of local excitations on one metal M*M ± MM*. The $1^{1,3}Eg$ and $1^{1,3}E_u$ states would be comprised of a combination where M* is a $d_{xz} \rightarrow d_{xy}$ state, or $(d_{z^2})^1(d_{yz})^1(d_{x^2})^2$ overall, while the $2^{1,3}E_g$ and $2^{1,3}E_u$ states would be comprised of a similar combination where M* is a $d_{xy} \rightarrow d_{xy}$ state. When we compare the calculated states to the observed spectra in a later section, it will be crucial to note that these states have a "doubly occupied" orbital on one of the metal sites—d_{xy} for $1^{1,3}E_g$ and d_{xy} (d_{yz}) for $2^{1,3}E_g$—in contrast to the δ–δ^* states or, for that matter, the $^3A_{2u}$ δ–δ^* state.

π–π^* States. A broad manifold of eight states extending from 3.8 to 7.5 eV all correspond to π–π^* excitations. A revealing analogy can be made between π–π^* states of the Re–Re quadruple bond and the observed π–π^* states of the triple bond in N_2 since the δ orbitals of Re species are not involved here. With the reduction in symmetry from $D_{\infty h}$ to D_{4h}, one can make a 1:1 correspondence between the states of the two molecules with essentially the same ordering of the multiplets as shown in Figure 4. In both cases the spin-forbidden triplet states $^3\Sigma_u^+$ ($^3A_{2u}$), $^3\Delta_u$ ($^3B_{1u}$, $^3B_{2u}$), and $^3\sum_u^-$ ($^3A_{1u}$) lie lowest, followed by the spin-allowed symmetry-forbidden singlet states $^1\Sigma_u^-$ ($^1A_{1u}$) and $^1\Delta_u$ ($^1B_{1u}$, $^1B_{2u}$), and followed by the dipole-allowed $^1\Sigma_u^+$($^1A_{2u}$) state at high energy (7.5 eV in $Re_2Cl_8^{2-}$).

Another complicated manifold, nominally associated with the $\pi\delta$–$\pi^*\delta^*$ double excitation, begins at energies 5.1 eV and above. This manifold may be viewed as the partner of the π–π^* states in the same sense that the $^{1,3}E_u$ $\delta\pi$–$\delta^*\delta^*$ states were partners of the $^{1,3}E_g$ π–δ^* states.

Table V. Electronic States of $Re_2Cl_8^{2-}$ with Spin-Orbit Coupling (g States)

excitation	dominant component	symmetry	energy, eV	% singlet
	1^1A_{1g}	A_{1g}	0.00	96
$\pi-\delta^*$	1^3E_g	A_{1g}	3.19	9
		A_{2g}	3.21	
		E_g	3.31	7
		B_{2g}	3.48	
		B_{1g}	3.49	
	1^1E_g	E_g	4.04	76
$\delta\delta-\delta^*\delta^*$	2^1A_{1g}	A_{1g}	3.61	87
$\delta-\pi^*$	2^3E_g	B_{2g}	4.28	
		B_{1g}	4.28	
		E_g	4.38	19
		A_{2g}	4.46	21
		A_{1g}	4.60	7
	2^1E_g	E_g	4.77	56
$\delta-\delta_{xy}$	1^1A_{2g}	A_{2g}	5.07	76
	1^3A_{2g}	A_{1g}	5.12	
		E_g	4.77	15
$\pi\delta-\pi^*\delta^*$	1^3A_{1g}	A_{2g}	5.24	6
		E_g	5.33	11
	1^3B_{1g}	E_g	5.57	6
		B_{1g}	5.59	
	3^1A_{1g}	A_{1g}	5.74	76
	1^3B_{1g}	E_g	5.94	
		B_{2g}	6.18	6
	1^3A_{2g}	A_{1g}	5.97	
		E_g	6.01	7
	1^1B_{2g}	B_{2g}	6.04	56
LMCT				
$a_{1u}-\delta^*$	2^3B_{1g}	B_{2g}, E_g	6.35-6.41	37
	1^1B_{1g}	B_{1g}	6.58	100
$b_{2u}-\delta^*$	4^3A_{2g}	A_{1g}, E_g	6.50-6.63	30
	2^1A_{2g}	A_{2g}	6.58	100
$e_u-\delta^*$	4^3E_g	A_{1g}, A_{2g}, B_{1g}, B_{2g}, E_g	7.04-7.34	12-60
	4^1E_g	E_g	7.35	86

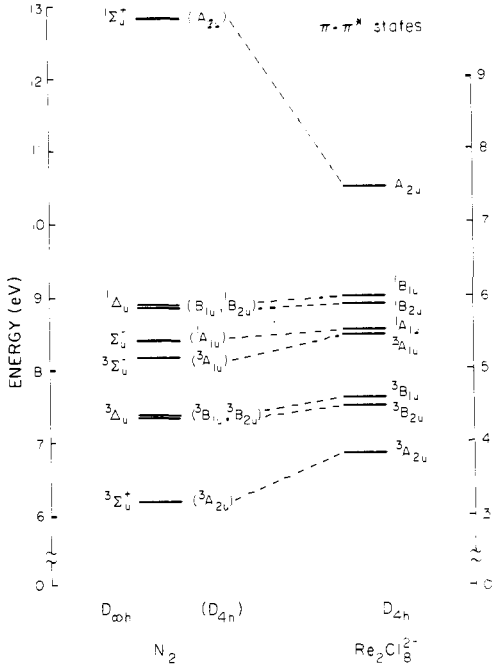

Figure 4. Comparison of the observed $\pi-\pi^*$ states in N_2 with the calculated $\pi-\pi^*$ states in $Re_2Cl_8^{2-}$ showing the correspondence with the reduction in symmetry from $D_{\infty h}$ to D_{4h}.

Other d–d States. At much higher energies, one finds states involving the σ bond of the dimer—the $\sigma-\delta^*$ $^3B_{1u}$ (5.26 eV) and $^1B_{1u}$ (5.30 eV) states and the $\sigma-\pi^*$ ^3E_g (5.91 eV) and ^1E_g (6.84 eV) states. A pure $\sigma-\sigma^*$ ($^{1,3}A_{2u}$) state could not be located, but the $\pi-\pi^*$ $^1A_{2u}$ state (7.5 eV) had strong contamination of $\sigma-\sigma^*$ character.

Ligand–Metal Charge-Transfer (LMCT) States. All of the states discussed thus far arise from excitations among the 5d orbitals of the Re ions in the dimer. The remaining important class of electronic states involves excitations from the occupied Cl 3p orbitals into the 5d metal orbitals—the ligand–metal charge-transfer (LMCT) bonds.

The theoretical treatment employed here is expected to yield less reliable results for the LMCT bands than for the d–d excitations. One factor contributing to this is the use of a minimal basis set (3s3p) to describe the ligand orbitals compared to the more flexible basis to describe the metal orbitals. In addition we have used ground-state orbitals to carry out the CI calculations. Charge-transfer excitations are typically associated with large rearrangements of orbitals when compared to ground-state orbitals. Whereas the ground state and all of the d–d excited states of $Re_2Cl_8^{2-}$ contained eight 5d electrons in the Re–Re bond, the LMCT states have nine 5d electrons in the d manifold, with correspondingly larger rearrangement effects. Finally, the use of a delocalized orbitals to describe the "hole" created on the ligand can neglect important polarization effects. A more realistic picture can often be obtained by using "broken symmetry" states to describe the excitation from one ligand that is later taken in appropriate symmetry combinations to obtain correct many-electron states.

All of the above effects will tend to produce electronic states that are too high in energy relative to the ground state, which we indeed observe (see Comparison with Experiment section). Nevertheless, the relative ordering and spacing of the LMCT states should be satisfactorily given by the calculations.

The highest occupied ligand orbitals have the energy ordering $...< 4e_g < 5e_g < 1a_{2g} < 3b_{2u} < 1a_{1u}$. When an electron from one of these orbitals is excited to the unoccupied δ^* ($2b_{1u}$) orbital, the following states arise (Table IV): $^{1,3}B_{1g} < {}^{1,3}A_{2g} < {}^{1,3}B_{2u} < {}^{1,3}E_u < {}^{1,3}E_u < ...$ (with the $^{1,3}B_{1g}$ state arising from the $1a_{1u} \rightarrow \delta^*$ excitation, etc.). From Table IV, the singlet–triplet splittings are of the order of 0.2 eV ($\sim$2000 cm^{-1}). The above ten states separated by nearly 1 eV.

Effects of Spin–Orbit Coupling

For heavy atoms such as Re, the effects of spin–orbit coupling become significant, and hence they have been incorporated with the framework discussed in the methods section. In this approach, the spin–orbit operator is diagonalized over the basis of many-electron states listed in Table IV. Since the matrix is diagonalized, the same answers will be obtained regardless of the coupling scheme (such as L–S vs. j–j in atoms) used. Since the spin–orbit states turn out to retain the basic parentage of the states in Table V, we shall treat the states in terms of this parentage. The results of the spin–orbit calculations are given in Tables V (g states) and VI (u states), where the excitation energies and dominant component (parentages) are given. Despite this nomenclature, all states of a given space–spin symmetry were allowed to interact in the spin–orbit calculations.

In the D_{4h} group, the spin wave functions transform as follows: singlet (S_0) $\sim$ A_{1g}, triplet (T_0) $\sim$ A_{2g}, triplet ($T_{\pm1}$) $\sim$ E_g. Thus the $^1A_{1g}$ ground state will have A_{1g} total symmetry in the double group while the $^3A_{2u}$ $\delta-\delta^*$ state will have states of A_{1u} and E_u symmetry after taking the direct product of space (A_{2u}) and spin (A_{2g}, E_g). The relative admixture of singlet character in each of the states is also given in Tables V and VI. The ground state is only slightly mixed with higher states:

$$1A_{1g} = 95.6\%\ (1^1A_{1g}) + 1.0\%\ (1^3A_{2g}) + 1.4\%\ (2^3E_g) + 1.0\%\ (4^3E_g) + ...$$

Higher states typically still have one dominant state but have larger admixtures; for example, the 1^1E_g ($\pi-\delta^*$) states becomes

$$2E_g = 75.6\%\ (1^1E_g\ \pi-\delta^*) + 4.9\%\ (1^3E_g\ \pi-\delta^*) + 16.8\%\ (2^3E_g\ \delta-\pi^*) ...$$

Overall, however, the spin–orbit splittings of the electronic-state

Table VI. Electronic States of $Re_2Cl_8^{2-}$ with Spin-Orbit Coupling (u States)

excitation	dominant component	symmetry	energy	% singlet	transition moment,[a] au with S-O	transition moment,[a] au without S-O
	(1^1A_{1g})	A_{1g}	0.00	(96)		
$\delta-\delta^*$	1^3A_{2u}	A_{1u}	0.85	2		
		E_u	0.87		7.5-3	
	1^1A_{2u}	A_{2u}	3.24	82	2.4-1	2.6-1
$\pi-\pi^*$	2^3A_{2u}	E_u	3.93		6.3-3	
		A_{1u}	3.99			
	1^3B_{1u}	B_{2u}	4.60	7		
		E_u	4.74		1.2-2	
	1^3B_{2u}	B_{1u}	4.67	10		
		E_u	4.82	15	1.9-2	
	2^3A_{1u}	A_{2u}	5.71			
		E_u	5.85		6.2-3	
	2^1A_{1u}	A_{1u}	5.81	80		
	1^1B_{2u}	B_{2u}	6.31	88		
	2^1B_{1u}	B_{1u}	6.34	92		
	2^1A_{2u}	A_{2u}	7.71	100	2.9-1	3.0-1
$\delta\pi-\delta^*\delta^*$	1^3E_u	A_{1u}	4.13			
		E_u	4.17	5	1.7-2	
		A_{2u}	4.21	16		
		B_{2u}	4.34			
		B_{1u}	4.34			
	1^1E_u	E_u	4.99	57	2.7-2	4.5-2
$\delta\delta-\delta^*\delta^*$	2^3E_u	B_{2u}	5.13			
		B_{1u}	5.15	5		
		E_u	5.36	6	1.3-2	
		A_{1u}	5.43	29		
		A_{2u}	5.56			
	2^1E_u	E_u	6.17	91	3.4-2	3.4-2
$\delta-\delta^*_{xy}$	$^3A_{1u}$	A_{2u}	5.05			
		E_u	5.18	6	1.8-2	
	$^1A_{1u}$	A_{1u}	5.09	89		
$\delta-\delta^*$	2^3B_{1u}	B_{2u}	5.46	4		
		E_u	5.49	3	1.9-2	
		B_{1u}	5.50	87		
LMCT						
$a_{2g}-\delta^*$	2^3B_{2u}	B_{1u} E_u	6.54		7.5-3	
	2^1B_{2u}	B_{2u}	6.76	98		
$4e_g-\delta^*$	3^3E_u	A_{1u}, A_{2u}, B_{1u}, B_{2u}, E_u	6.62-6.95	7-14	4.4-3	
	3^1E_u	E_u	7.08	61	5.2-1	6.3-1
$3e_g-\delta^*$	4^3E_u	A_{1u}, A_{2u}, B_{1u}, B_{2u}, E_u	6.82-6.92	4	1.9-1	
	4^1E_u	E_u	7.16	99	9.1-1	9.5-1

[a] Transition moments expressed in au (1 au = 0.527×10^{-8} cm) as $l.n$-m to denote $l.n \times 10^{-m}$.

manifolds (0.1–0.4 eV) are comparable to or smaller than the singlet–triplet splitting of the states without spin–orbit splitting (0.1–0.8 eV). Thus we still refer to the states as being primarily ^3E_g ($\pi-\delta^*$), ^3E_g ($\pi-\delta^*$), etc.

Transition Moments

The dipole-allowed transition moments from the $^1A_{1g}$ ground state are also shown in Table VI from calculations with and without spin–orbit coupling. In the latter case, only $^1A_{2u}$ (z or $\parallel$ polarization) and ^1E_u (x, y, or $\perp$ polarization) states have nonzero transition moments. The transition moments can be classed into (1) the strong LMCT transitions (0.6–0.9 au), (2) the somewhat weaker $\delta-\delta^*$ and $\pi-\pi^*$ excitations ($\sim$0.3 au), and (3) the weak $\delta\pi-\delta^*\delta^*$ and $\delta\delta-\delta^*\delta^*$ excitations (0.04 au) where 1 au = 0.529×10^{-8} cm. That the latter states have any intensity at all is at first sight surprising in view of the fact that they are both nominally double excitations from the ground state and thus should not be coupled by the one-electron dipole operator. These nonzero transition moments are another manifestation of the fact, repeatedly stressed here, that the states are not really well described by a single configuration. In this case, the large admixture of the $(\sigma)^2(\pi)^4(\delta^*)^2$ configuration in the nominal "$(\sigma)^2(\pi)^4(\delta)^2$" ground state accounts for making allowed otherwise-forbidden two-electron transitions. The $\pi\delta-\delta^*\delta^*$ and $\delta\delta-\delta^*\pi^*$ ^1E_u states, which are one-electron transitions from the lesser $(\sigma)^2(\pi)^4(\delta^*)^2$ ground-state configuration, in this manner acquire their intensity. (Only qualitative importance should be given to the computed transition moments since any properties calculated by using pseudoorbitals should really be corrected to incorporate the orthogonality effects of the core orbitals.)

When spin–orbit coupling is included, triplet states that were originally spin-forbidden transitions from the ground state can acquire intensity from admixtures of singlet character. Similarly, the slight admixture of triplet character into the ground state will also contribute to intensities of singlet–triplet transitions. For an allowed transition, the excited state must possess either A_{2u} ($\parallel$) or E_u ($\perp$) total symmetry. All triplet states having u spatial symmetry in D_{4h} will have an E_u component, since the direct product of any state with u spatial symmetry with E_g spin symmetry produces an E_u representation.

As shown in Table VI, the effect of spin–orbit coupling is to induce weak transition moments to triplet states, while the allowed transitions are only slightly affected in intensity. Generally, the spin–orbit-allowed singlet-triplet transitions have transition moments an order of magnitude smaller (and hence intensities 10^{-2} smaller) than the strongly allowed LMCT or $\delta-\delta^*$ excitations. The E_u component of the low-lying $\delta-\delta^*$ $^3A_{2u}$ state has an extremely small moment (7.5×10^{-3} au) and hence is unlikely to be seen in direct absorption or emission studies.

Corrections to Calculated Excitation Energies

For the purposes of comparing to experiment, the computed values of the excitation energies have been corrected to allow for additional correlation effects not explicitly included in the calculations:

(1) Since a nearly constant lowering of 0.4 eV was discussed in going from the smaller GVB-CI to POL-CI calculations (see Table II), all excitation energies from Tables IV, V, and VI were lowered by this increment to give the values in Table VII.

(2) The most definitively assigned excited state, on the basis of polarization studies at low temperature,[32] is the $^1A_{2u}$ $\delta-\delta^*$ state at 14 600 cm^{-1} (1.8 eV). At the POL-CI level this state is found to be nearly 1 eV higher at 2.85 eV. We associate this residual 1-eV discrepancy to the atomic correlation energy of a doubly occupied d orbital on one of the metal atoms in the GVB description of the $^1A_{2u}$ state (see above). This intrapair atomic correlation energy is absent in the ground state, which can be considered conceptually as two high-spin d^4 configurations on each center coupled into four bonds of varying strength. In contrast to the ground $^1A_{1g}$ state and $\delta-\delta^*$ $^3A_{2u}$ excited state having a local $(d_{z^2})^1(d_{xz})^1(d_{yz})^1(d_{xy})^1$ configuration on each metal, the other excited states involving the δ^* or π^* orbitals all have local configurations with a doubly occupied d_{xy} or d_{xz} orbital on one metal. In recent studies of relativistic and correlation effects in transition-metal atoms,[19] we have found the intrapair correlation energy associated with double occupying a d orbital can be at least 1 eV in the second and third transition series and 3 eV in the first transition series.

Thus, all excited states are reported with an additional 1.0-eV downward energy correction. The only exceptions are the $^3A_{2u}$ $\delta-\delta^*$ and the $^{1,3}A_{2g}$ and $^{1,3}A_{1u}$ $\delta-\delta'$ states, which retain singly occupied atomic orbitals on each site.

Comparison with Experimental Spectra

These calculations reveal a rich and complex spectrum of excited states, the details of which have only partially been outlined by the numerous experimental studies to date.[4,27,29-34] The electronic states are summarized in Table VII along with the main peaks in the observed spectrum and their assignments to date. The

(32) C. D. Cowman and H. B. Gray, *J. Am. Chem. Soc.*, **95**, 8177 (1973).
(33) W. K. Bratton, F. A. Cotton, M. Debeau, and R. A. Walton, *J. Coord. Chem.*, **1**, 121 (1971).
(34) R. J. H. Clark and M. L. Franks *J. Am. Chem. Soc.*, **98**, 2763 (1976).

Table VII. Summary of Calculated and Experimental Results for the Low-Lying Electronic States of $Re_2Cl_8^{2-}$

state	dominant excitation	calcd excitation energies with corrections, eV: without S-O	with S-O	calcd transition moment,[a] au	exptl peaks: E (eV)	ν, cm^{-1}	int[b]	pol	previous assignmt
1^1A_{1g}		0.0	0.0						
1^3A_{2u}	δ-δ^*	0.4	0.4	7.5-3 ($\perp$)					
1^1A_{2u}	δ-δ^*	1.8	1.8	2.4-1 ($\parallel$)	1.8	14 000	s	$\parallel$	$^1A_{2u}$ (δ-δ^*)
1^3E_g	π-δ^*	1.8	1.8-2.1						
2^1A_{1g}	$\delta\delta$-$\delta^*\delta^*$	2.0	2.2						
1^1E_g	π-δ^*	2.5	2.6		2.2	17 700	w	$\parallel$, $\perp$	^1E_g (δ-π^*)
2^3A_{2u}	π-π^*	2.4	2.6	6.3-3 ($\perp$)					
1^3E_u	$\pi\delta$-$\delta^*\delta^*$	2.6	2.7-2.9	1.7-2 ($\perp$)	2.6	21 000	w	$\perp > \parallel$	$^1A_{1u}$ (δ-$\delta_{x^2-y^2}$)
2^3E_g	δ-π^*	2.8	2.9-3.2						
1^3B_{1u}	π-π^*	3.1	3.2	1.2-2 ($\perp$)					
1^3B_{2u}	π-π^*	3.2	3.3	1.2-2 ($\perp$)					
2^1E_g	δ-π^*	3.4	3.4		2.93	23 600	w	$\perp$	^1E_g (π-δ^*)
1^1E_u	$\pi\delta$-$\delta^*\delta^*$	3.4	3.6	1.7-2 ($\perp$)					
2^3E_u	$\delta\delta$-$\delta^*\pi^*$	3.6	3.7-4.1	2.3-2 ($\perp$)					
2^3A_{1u}	π-π^*	4.0	4.4	6.2-3 ($\perp$)					
2^1A_{1u}	π-π^*	4.1	4.4						
2^1E_u	$\delta\delta$-$\delta^*\pi^*$	4.4	4.8	3.4-2 ($\perp$)					
$1^{1,3}A_{2g}$	δ-$\delta_{x^2-y^2}$	4.4	4.6						
$1^{1,3}A_{1u}$	δ-$\delta_{x^2-y^2}$	4.4	4.6	1.8-2 ($\perp$)					
1^1B_{2u}	π-π^*	4.5	4.9						
2^3B_{2u}	LMCT a_{2g}-δ^*	5.1	5.1	7.5-3 ($\perp$)					
2^1B_{2u}		5.3	5.3						
3^3E_u	LMCT e_g-δ^*	5.5	5.2-5.5	4.4-3 ($\perp$)	3.5	28 200	w		^3E_u (LMCT)
3^1E_u		5.7	5.7	5.2-1 ($\perp$)	3.8	30 600	s	$\perp$	^1E_u (LMCT)
4^3E_u	LMCT e_g-δ^*	5.5	5.4-5.5	1.9-1 ($\perp$)					
4^1E_u		5.8	5.8	9.1-1 ($\perp$)					
2^1A_{2u}	π-π^*, σ-σ^*	6.3	6.3	3.1-1 ($\parallel$)	4.9	39 500	s	$\parallel$	π-π^*

[a] Table VI, footnote *a*. [b] Intensities: strong (s), weak (w).

calculated transition moments are given as a qualitative guide to relative intensities for the dipole-allowed states. (This treatment includes spin–orbit coupling as the only mechanism whereby normally forbidden states such as triplet states can acquire intensity. Vibronic mixing mechanisms can be equally important in enhancing the intensities of forbidden states, but an analysis of vibronic effects would require detailed information on the transition moments as a function of nuclear geometry along various vibrational modes and is beyond the scope of this paper.)

In Table IX (supplementary material), the theoretical excitation energies are given both with and without spin–orbit coupling. Ranges of energies are often given for the spin–orbit components (for more detailed information see Tables V and VI). As discussed in the previous section, for the sake of comparison with experiment, the theoretical excitation energies have been corrected to align the δ–δ^* $^1A_{2u}$ state with the observed peak at 1.8 eV (14 000 cm^{-1}) since the best calculations apparently overestimate this energy by about 1 eV. We would expect this semiempirical correction to apply equally well for the other d–d excitations in Table VII.

The other major landmark of the UV spectrum of $Re_2Cl_8^{2-}$ is the strong peak at 3.8 eV (30 600 cm^{-1}) assigned to ligand–metal charge-transfer (LMCT) bands.[4] For the reasons detailed earlier, the calculations are not expected to provide quantitative information on the location of this band. Indeed the 4e → δ^* ^1E_u state occurs at 5.7 eV (Table VII) with a large calculated transition moment (0.5 au), but considerably higher in energy than the observed peak.

Between the strong 14 000 cm^{-1} (δ–δ^* $^1A_{2u}$) peak and the 30 000 cm^{-1} (LMCT) peak, Trogler et al.[4,25] observed a number of weaker bands. They made assignments for these bands on the basis of low-temperature polarization studies and with the aid of the available theoretical calculations at the time, of which the most extensive were the Xα scattered wave (Xα-SW) results of Mortola et al.[8] The earlier discussions about the highly correlated nature of electronic states in multiple metal–metal bonds and the limitations of single-configuration descriptions of the states suggest that Xα-SW results for metal–metal bonds be viewed with caution. Our results show a much richer manifold of states in this region than previously suspected. We do find π–δ^* ^1E_g and δ–π^* ^1E_g states at 2.5 and 3.4 eV, respectively, in close agreement with the peaks at 2.2 and 2.9 eV assigned by Trogler et al. to ^1E_g states. The peaks were presumed to have the relative ordering δ–π ^1E_g* < π–δ ^1E_g* on the basis of the Xα-SW results, whereas the present results indicate the reverse is true.

A host of other electronic states also exist in this region and may have been glimpsed in the spectra. A third weak progression at 2.6 eV was tentatively assigned to an δ–δ $^1A_{1u}$ state. The present calculations find this state to occur at much higher energies (4.4 eV), however, but to predict eight additional electronic states between 1.8 and 3.4 eV not counting the two ^1E_u states. These include π–π^* triplet states as well as nominally doubly excited $\pi\delta$–$\delta^*\delta^*$ ^3E_u and ^1E_u states. The latter type can have significant intensity, as mentioned before, because of the presence of large $\delta\delta$–$\delta^*\delta^*$ excitations in the ground state. In fact, the transition moment to the $\pi\delta^*$–$\delta^*\delta^*$ ^1E_u state is only one order of magnitude lower than the calculated moment for the δ–δ^* $^1A_{2u}$ transition.

The weak band 0.3 eV below the strong LMCT peak does in fact appear to be the ^3E_u state partner of the ^1E_u dipole-allowed LMCT state calculated to lie 0.2–0.5 eV below the main peak. Finally, at much higher energies, we find the strongly mixed π–π^* and σ–σ^* $^1A_{2u}$ state at 6.3 eV, which apparently corresponds to the strong peak at 4.9 eV with z polarization consistent with a $^1A_{2u}$ state.

There appears to be no experimental confirmation yet of the very low-lying δ–δ^* $^3A_{2u}$ state calculated to lie about 4000 cm^{-1} above the ground state with a very small transition moment (0.008 bohr) for the A_{1g} ($^1A_{1g}$) → E_u ($3A_{2u}$) spin–orbit-allowed transition. Originally it was suspected to lie slightly below the δ–δ^* $^1A_{2u}$ state from emission studies,[29] but these peaks have been now attributed to progressions in the torsional mode along the pathway toward the staggered D_{4d} structure.[30] Indeed, these calculations predict the $^1A_{2u}$ state to gain at least 2000 cm^{-1} in stabilization energy (Figure 2) upon twisting to the staggered form. The generalized valence bond description of the δ–δ^* states in terms of weakly interacting δ orbitals on each metal leads directly to the expectation of a low-lying δ–δ^* $^3A_{2u}$ state. This contrasts with the usual expectation in MO theory of finding a triplet state at only slightly lower energy than its singlet counterpart.

The only possible evidence to date for the low-lying $^3A_{2u}$ state in quadruple metal–metal bonds is the work of Clark and Franks,[35] who observed a weak absorption at 6250 cm^{-1} (0.8 eV) in certain $Mo_2Cl_8^{4-}$ salts that they ascribed to $^1A_{1g} \rightarrow {}^3A_{2u}$ absorption. In $Re_2Cl_8^{2-}$ itself, the $^3A_{2u}$ state (calculated to lie at 4000 cm^{-1}) has apparently remained totally elusive.

Summary

A comprehensive theoretical study of the electronic states of the quadruply bonded $Re_2Cl_8^{2-}$ species has revealed a rich spectrum of states below 6 eV (50 000 cm^{-1}). The nature of these states is discussed in terms of the orbitals involved in the excitations. The weak coupling between the metal orbitals of the δ bond in particular necessitates a multiconfiguration description in terms of MO's, and a valence bond interpretation can often yield insights into the nature of the states. Of the states arising from δ–δ^* excitations, the $^1A_{2u}$ state (calculated 2.8 eV; observed 1.8 eV) has been well characterized experimentally, while the $^3A_{2u}$ (calculated 0.40 eV) and 2^1A_{1g} (calculated 3.22 eV) apparently have oscillator strengths too weak to be observed (cf. Tables II and VII). All three δ–δ^* excited states should undergo torsional distortions toward D_{4d} geometries. A large number of other weakly absorbing and forbidden states are found to lie between the strong $^1A_{2u}$ absorption and the LMCT states at 3.8 eV—a region that has been the subject of detailed spectroscopy studies.[4,25]

Acknowledgment. We thank Professor Harry Gray for the hospitality of his group and for useful discussions on the nature of the absorption and emission spectra of $Re_2Cl_8^{2-}$. We also thank Professor F. A. Cotton and Dr. Bruce Bursten for helpful discussions and for results of their unpublished absorption spectra and theoretical calculations prior to publication. This work was carried out under the auspices of the U.S. Department of Energy.

Registry No. $Re_2Cl_8^{2-}$, 19584-24-8.

Supplementary Material Available: Gaussian basis sets and effective core potentials used in these calculations (Tables VIII and IX) (2 pages). Ordering information is given on any current masthead page.

(35) R. J. H. Clark and M. L. Franks, *J. Am. Chem. Soc.*, **97**, 2691 (1975).

Overlap Control and Stability of Polyhedral Molecules. *closo*-Carboranes

Eluvathingal D. Jemmis

Contribution from the School of Chemistry, University of Hyderabad, Central University P.O., Hyderabad 500 134, India. *Received January 20, 1982*

Abstract: *closo*-Carboranes that can be formally divided into rings and caps follow a six-electron rule. The relative stability of various isomers within a given carborane depends on the size of the ring on which the polyhedral structure is based. With three- and four-membered rings the CH group fits in as the best cap; the overlap of the orbitals of CH with the orbitals of three- and four-membered borocycles is favorable. Thus 1,5-$C_2B_3H_5$ is more stable than 1,2-$C_2B_3H_5$. The BH group with more diffuse orbitals overlaps better with the orbitals of a five-membered ring; 1,7-$C_2B_5H_7$ is less stable than 1,2-$C_2B_5H_7$, which, in turn, is less stable than 2,4-$C_2B_5H_7$. The orbitals of BH are not diffuse enough to overlap favorably with the orbitals of a six-membered ring; $C_2B_6H_8$ prefers a dodecahedron to a hexagonal bipyramid. Caps with more diffuse orbitals such as BeH, Li, and transition-metal fragments should stabilize polyhedra based on six-membered rings.

The *closo*-carboranes represent one of the most studied sets of polyhedral molecules.[1] Despite the various electron-counting rules[2] and theoretical studies[3] available, the factors controlling the isomer stabilities of carboranes are not yet understood. Consider the series of *closo*-carboranes given in Figure 1. **1a**, the trans isomer (**1**,5-$C_2B_3H_5$), is more stable than the 1,2- and 2,3-isomers.[1a,3] Similarly **2a** (1,6-$C_2B_4H_6$) is more stable than **2b**. But **3a** is the least stable of the four $C_2B_5H_7$ isomers.[3] Carboranes based on six-membered rings as in **4** are unknown; $C_2B_6H_8$ prefers the dodecahedron, **5**, compared to the hexagonal bipyramid, **4**.[4] In contrast to the propensity of polyhedra based on four- (**6**) and five- (**7**) membered rings (Figure 2), those based on six-membered rings (**8**) are absent among carboranes.[1] There is no consistent set of explanations for these observations. The suggestion that the more electronegative atoms prefer to be farthest apart in the most stable isomer works in **1**, **2**, **6**, and **7** but fails in **3**.[1a] The postulate that the position isomer having the largest number of B–C bonds will be most stable within a given set of isomers also does not work uniformly.[1b] The empirical observation that carbon prefers a site of less coordination seems to explain most of them, but a theoretical explanation for this preference is lacking.[2a] The absence of carboranes of the types **4** and **8** also remains a puzzle. We present here a criterion based on overlap of orbitals to determine relative isomer stabilities of polyhedral carboranes.

Carboranes considered in this paper can be formally constructed from caps and rings. The electronic structure of carboranes can be then understood by a six-electron rule. Let us consider **2a**, which has a four-membered borocycle, B_4H_4, with two CH caps attached from either side. With the assumption of two-center

(1) (a) Grimes, R. N. "Carboranes"; Academic Press: New York, 1970. (b) Muetterties, E. L., Ed. "Boron Hydride Chemistry"; Academic Press: New York, 1975. (c) Muetterties, E. L.; Knoth, W. H. "Polyhedral Boranes"; Marcel Dekker: New York, 1968. (d) Purcell, K. F.; Kotz, J. C. "Inorganic Chemistry"; W. B. Saunders: Philadelphia, 1977; Chapter 18.

(2) (a) Williams, R. E. *Adv. Inorg. Chem. Radiochem.* **1976**, *18*, 67. (b) Wade, K. *Ibid.* **1976**, *18*, 1. (c) Rudolph, R. W.; Pretzer, W. P. *Inorg. Chem.* **1972**, *11*, 1974. (d) Mingos, D. M. P. *Nature (London)* **1972**, *236*, 99. (e) Lipscomb, W. N. "Boron Hydrides"; W. B. Benjamin: New York, 1963.

(3) (a) Stone, A. J.; Alderton, M. J. *Inorg. Chem.* **1982**, *21*, 2297. (b) Dewar, M. J. S.; McKee, M. L. *Ibid.* **1980**, *19*, 2662. (c) Dixon, D. A.; Kleir, D. A.; Halgren, T. A.; Hall, J. H.; Lipscomb, W. N. *J. Am. Chem. Soc.* **1977**, *99*, 6226. (d) Bicerano, J.; Marynick, D. S.; Lipscomb, W. N. *Inorg. Chem.* **1978**, *17*, 3443. (e) King, R. B.; Rowray, D. H. *J. Am. Chem. Soc.* **1977**, *99*, 7834. (f) Hoffmann, R.; Lipscomb, W. N. *J. Chem. Phys.* **1962**, *36*, 2179, 3489.

(4) (a) Dunks, G. B.; Hawthorne, M. F. *Inorg. Chem.* **1968**, *7*, 1038. (b) Williams, R. E.; Gerhard, F. J. *J. Am. Chem. Soc.* **1965**, *87*, 3513. (c) Garrett, P. M.; Smart, J. C.; Ditta, G. S.; Hawthorne, M. F. *Inorg. Chem.* **1969**, *8*, 1907.

0002-7863/82/1504-7017$01.25/0